Research article

Environmental controls on air pollution dispersion over Richards Bay, South Africa

Mark R Jury [1, 2*]

[1]Department of Geography and Environmental Studies, University of Zululand, KwaDlangezwa, South Africa
[2]Physics Department, University of Puerto Rico Mayagüez, USA
*Corresponding author: mark.jury@upr.edu

Received: 10 January 2024 - **Reviewed:** 4 April 2024 - **Accepted:** 23 April 2024
https://doi.org/10.17159/caj/2024/34/1.17581

Abstract

Air pollution dispersion over Richards Bay, South Africa is studied using satellite, reanalysis and in-situ measurements. Near-surface concentrations of trace gases and particulates reach high concentrations under dry stable 'berg' winds. Temporal records of CO, NO_2, O_3, $PM_{2.5}$, SO_2 (2000-2023) exhibit no trend and short-term dose excedances of individual pollutants are rare and confined to winter mornings. Regional point-to-field correlation maps of a Richards Bay winter air pollution index found that anomalous warming of the west Indian Ocean accelerates the jet stream over Madagascar and pulls smoke- and dust-laden north-westerly winds across the South African plateau, implicating long-range transport. At daily and hourly time scales dewpoint temperature and boundary layer height best indicate changes in local air pollution dispersion that impact respiratory health. A case study of 15-17 June 2021 revealed a 10°C thermal inversion caused by negative sensible heat fluxes of -40 W/m^2 through the night, leading to SO_2 concentrations above 100 ppb in the morning along the main access road (28.8°S, 32°E). Poor dispersion seldom happens in the summer when turbulent mixing and rainfall cleanse the air.

Keywords

Richards Bay, South Africa, meteorology, air pollution dispersion

Introduction

Urban, industrial and agricultural activities generate wealth but often incur atmospheric emissions that can degrade ecosystems and impair respiratory health (Akimoto 2003, World Bank 2016, WHO 2021). Manufacturing and power generation in the South African Highveld emit ~10^4 Tons km^{-2}/yr of carbon monoxide (CO), nitrogen dioxide (NO_2), ozone (O_3), sulfur dioxide (SO_2) and fine particulates ($PM_{2.5}$), which lead to acidic deposition (Josipovic et al. 2011, Conradie et al. 2016, Jury 2017, Tularam et al. 2021). Local pollutants are joined by regional smoke plumes from tropical deforestation and Kalahari dust plumes (Piketh et al 1999, Silva et al. 2003, Battachan et al. 2012, Ma et al. 2013). As emissions disperse under sunlight, photochemical reactions generate O_3 and reduced visibility. In contrast with the interior plateau, KwaZulu-Natal has a humid climate underpinned by an anticyclonic circulation pulsed by eastward moving troughs (Preston-Whyte & Tyson 1988, Jury & Freiman 2002). Although marine winds of ~ 7 m/s tend to disperse 10^5 Tons/year of pollutants along the coast near Durban (Scorgie 2012, Gopaul et al. 2019), unhealthy concentrations prevail about 5% of the time in the dry winter season when emissions are trapped beneath a thermal inversion (Simpson & McGee 1996, Diab & Matooane 2003, Ramsay 2010, Jury & Buthelezi 2022).

South Africa's northeast coast is an increasingly popular destination due to its year-round warm weather. A new road network connecting Maputo and Durban has increased trade and tourism in the Zululand area, leaving small areas of wealth surrounded by rural poverty. Richards Bay (28.8°S, 32°E) has evolved from a fishing village to a coastal resort in the 1950s (Aniruth 1997, Cubbin 1998). In the 1970s a 60 km^2 deep-water port was constructed for the export of minerals and industrial products amounting to ~100 million Tons/year. Richards Bay's maritime trade and supporting industries employ more than 10,000 people making up ~ 50% of formal jobs, whose revenue contributes to a municipal budget of ~ R1400 million/year. On-going efforts to diversify the economy toward tourism have included a waterfront marina and beaches, and lakefront golf course and rustic lodges. Environmental use of natural amenities is at odds with the city's role as an industrial hub (Magi and Nzama, 2002). The area is susceptible

to pollution from land- and water-borne pathways that seep into recreational and residential areas. Atmospheric emissions of ~7000 Tons/day of CO_2 and ~100 Tons/day of CO, $PM_{2.5}$, O_3, SO_2, NO_2, hydrogen fluoride and ammonia tend to accumulate during the dry winter season (May-Aug) under weak westerly winds (Jury 2000, Petzer et al. 2008). One-quarter of the 100,000 downtown residents make clinical visits every year for allergic and asthmatic reactions (Jaggernath 2013, Okello et al. 2020). Airborne pollutants are monitored by the Richards Bay Clean Air Association and reported to the South Africa Air Quality Information System (SAAQIS). Although dose exceedances are rare for SO_2 and particulates (Okello et al. 2018), sinus allergies are common and environmental stress continues amidst an industrial agenda. Historical development plans that put major industries one kilometer from the commercial centre (Figure 1a-c) can't be undone, so the city maintains narrow buffer zones between industry and urban areas.

Richards Bay has a southeast facing coast swept by warm currents and stormy seas. The sub-tropical weather is changeable and humid winds create wetlands dotted by lakes. Microplastics are dense (>2%) near the waterfront and harbour effluents infiltrate the seafloor sediment (Mehlhorn et al. 2021). The port is bound by jetties that prevent the northward flux of sand (Mitchell et al. 2005), so beaches are retreating and limit development options.

Point source emissions form narrow plumes that disperse over space and time. Short-term exposure has marginal impact, but long-term dose maps can be used to link atmospheric dispersion to respiratory health risk. In that regard, satellite measurements of near-surface air pollutants (Burrows et al. 2011, Korhonen et al. 2014, Sundström et al. 2015, Krotkov et al. 2016) can be assimilated with in-situ observations and emission inventories by sophisticated air chemistry models to enable the study of trace gases and particulates over urban areas. Here, the following questions are addressed: i) what is the extent of local air pollution from hourly to annual time scales? ii) how do the winter climate and local weather influence air pollution concentrations? iii) are distant pollution sources involved in local episodes, iv) what mitigating actions can be taken to reduce health risks?

Data and Methods

MERRA2 air chemistry data assimilation (Molod et al. 2015, GEOS-5 2016, Gelaro et al. 2017, Randles et al. 2017) provides monthly surface CO, O_3, $PM_{2.5}$ and SO_2 concentrations at ~ 50 km resolution from Jan 2000 – Nov 2023. An air pollution index was formed by summing the four values (ppb) at the grid point 28.8°S, 32°E. Daily air constituents NO_2 and SO_2 derive from OMI satellite (Lamsal et al. 2014) and $PM_{2.5}$ from MERRA2

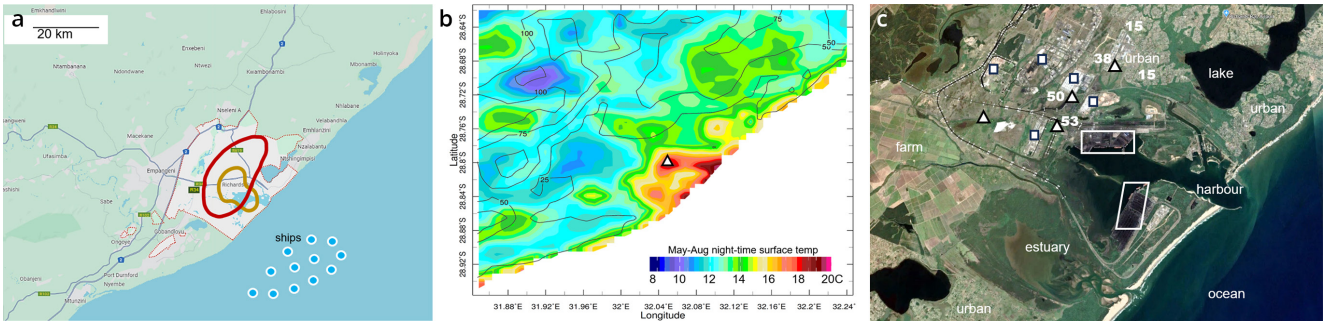

Figure 1: *a) Map of Richards Bay area and main roads, with dots representing awaiting ships (in Jan 2024), and red / orange outlining high SO_2 / PM_{10} concentration (adapted from Petzer et al. 2008). b) winter mean nocturnal land surface temperature at 1 km resolution from infra-red satellite with elevation contours. c) Close-up satellite photo of the harbour with weather and air pollution stations Δ, point-source emissions □, coal loading zones outlined white, numbers refer to average of daily maximum SO_2 (Petzer et al. 2008).*

Table 1: *Datasets used in the analysis*

Acronym	Name	Space, time resolution	Quantity
CALIPSO	Cloud-Aerosol Lidar & Infrared Pathfinder Satellite Observation	1 km on N-S slice, weekly	Particulate density
ERA5	European Community reanalysis version 5	25 km, daily, monthly	Near-surface meteorology
HYCOM	Hybrid coordinate ocean model reanalysis v3	10 km daily	Sea surface temperature, ocean current
HYSPLIT	Hybrid Lagrangian Trajectory model	25 km	Long-range transport via near-surface airflow
MERRA2	Modern era reanalysis for research & applications with GEOS-5 air chemistry	50 km, daily, monthly	Near-surface CO, O_3, $PM_{2.5}$, SO_2
MODIS	Infrared and visible band radiometer	1 km	Surface temperature, vegetation, fires
OMI	Ozone Monitoring Instrument	25 km, twice daily	Near-surface NO_2 & SO_2 concentration
SAAQIS	South African air quality information system, RBCAA monitoring	Station, hourly	Surface $PM_{2.5}$, PM_{10}, SO_2 conc, meteorology
SAWS	South African Weather Service	Radiosonde, surface obs.	Air & dew temp, wind velocity, air pressure

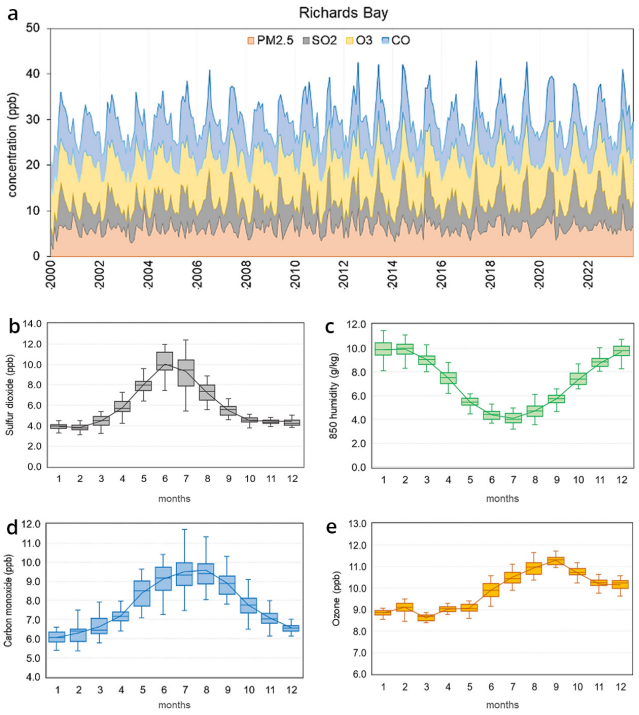

Figure 2: *a) Temporal record of monthly MERRA2 assimilated air pollution constituents in Richards Bay, plotted in aggregate. Box-whisker mean annual cycle of monthly: b) SO_2, c) 850 hPa specific humidity, d) CO, and e) O_3.*

at 28.8°S, 32°E in the period Oct 2004 – Nov 2023. Gaps in polar-orbiting satellite coverage were reduced by application of a 3-day running maximum. Hourly $PM_{2.5}$, PM_{10}, SO_2 and meteorology measurements in Richards Bay derive from in-situ stations (Fig 1c) reported to SAAQIS. MODIS satellite infrared and visible band radiance was analyzed for night-time thermal patterns, vegetation fraction and fire locations at 1 km resolution.

The monthly, daily and hourly near-surface meteorological data at 28.8°S, 32°E were derived from the 25 km resolution European Reanalysis v5 (ERA5, Hersbach et al. 2020) and include: air and dewpoint temperature, wind velocity, specific humidity, sensible heat flux and boundary layer height (BLH) or mixing depth. Surface values are preferred given the low elevation of Richards Bay (Fig 1b), but to quantify transport and dispersion the 925 hPa (~700 m) winds and 850 – 1000 hPa (1500 – 10 m) temperature difference 'delta T' were calculated. Hourly analysis of air pollution events utilize in-situ weather station data: air and dewpoint temperature, air pressure and solar radiation, wind speed and direction. Table 1 summarizes the dataset characteristics. One limitation is the ~50 km resolution of MERRA2, which makes it too coarse to identify the dispersion footprint of Richards Bay, necessitating finer scale products and in-situ measurements.

The mean annual cycle of monthly CO, O_3, SO_2 and 850 hPa humidity was calculated to identify the winter months May-August as most important (Shikwambana & Sivakumar 2019). Statistical pearson-product cross-correlations were calculated between the satellite/model air constituents and independent ERA5 meteorology time series at Richards Bay. The various records cover 288 months (2000-2023), 7000 days (2004-2023), and 2950 hours (May-Aug 2021). Significance at 95% confidence was evaluated according to the degrees of freedom (deflated for persistence). The appropriate thresholds are $r \geq |0.41|$ monthly, $|0.17|$ daily, and $|0.21|$ hourly. Pulsing of the weather was revealed by application of wavelet spectral analysis to the daily time series of ERA5 dewpoint temperature. Dispersion footprints were mapped using OMI satellite NO_2 and MERRA $PM_{2.5}$ data during the winter. The daily satellite NO_2 and SO_2 concentration record at Richards Bay was used to identify the winter of 2021 for further study. Maps of satellite NO_2 and height sections of CO concentration were calculated and compared with wind observations from Durban airport. The mean diurnal cycle was calculated from hourly in-situ SO_2 and weather data, and surface airflow patterns were analyzed by vector averaging May-Aug 2021.

To understand the influence of inter-annual climate variability, the Richards Bay winter air pollution time series was correlated with regional fields of ERA5 sea level air pressure, 500 hPa geopotential height, sea surface temperature and NOAA satellite net outgoing longwave radiation (OLR) representing atmospheric moisture (May-Aug 2000-2023). Ranking the air pollution index time series, the top-20 winter months were identified and composite atmospheric circulation anomalies were calculated from 1000 to 100 hPa (0-12 km height).

From the Richards Bay SO_2 time series an air pollution event 15-17 June 2021 was identified for detailed study of local weather using in-situ observations. A radiosonde profile at Durban airport 02:00 16 June 2021 was analyzed for vertical structure of wind, air temperature and dewpoint 1000 – 700 hPa (0-3 km). It is located 150 km southwest of Richards Bay and may be considered representative of KwaZulu-Natal. Regional smoke plumes were analyzed from MERRA2 assimilation 15-17 June 2021, and satellite fire density (FIRMS 2023) and vegetation fraction were analyzed. Lastly, a particulate event was analyzed for 4-5 July 2022. Local measurements and a north-south height section of CALIPSO satellite particulates (Winkler et al. 2007) were analyzed. HYSPLIT back-trajectories were calculated (Stein et al. 2015) to identify long-range transport of dust and smoke plumes from distant sources and local hourly weather data were obtained on wind speed and direction, sensible heat flux and boundary layer height.

Results

Geography and climate

The coastal plains near Richards Bay align in a SW-NE axis and rise slowly inland to the hills of Zululand. The Mhlatuze River valley forms a basin around the harbour (Fig 1a-c). Average winter night-time surface temperatures decrease westward from 20° to 10°C just 40 km inland. Over the city, nocturnal temperatures remain elevated above 16°C, constituting the urban heat island. Figure 1a-c illustrates emission and station

Table 2: *Simultaneous cross-correlation of MERRA2 surface air constituents and ERA5 meteorology variables over Richards Bay: a) monthly 2000-2023, b) daily 2004-2023, c) hourly May-Aug 2021; bold values significant at 95% confidence. Meteorological parameters are surface except: 925 = 0.7 km, 850 = 1.5 km, 700 = 3 km elevation; abbreviations: air poll. = sum of all constituents, p.evap = potential evaporation, w.speed (wind), L.H.F. and S.H.F. = latent and sensible heat flux, U V W = east, south and vertical airflow, q = specific humidity, T dew (dewpoint), delta T = lapse rate (+ stable), B.L.H. = boundary layer height.*

monthly	air poll	$PM_{2.5}$	SO_2	O_3	CO
$PM_{2.5}$	0.63				
SO_2	0.88	0.36			
O_3	0.52	0.14	0.23		
CO	0.87	0.27	0.77	0.56	
rain	-0.53	-0.19	-0.52	-0.26	-0.55
pot.evap	-0.60	-0.13	-0.74	-0.14	-0.58
w.speed	-0.04	0.01	-0.32	0.53	0.01
L.H.F.	-0.55	-0.18	-0.49	-0.35	-0.63
S.H.F.	-0.55	-0.18	-0.65	-0.13	-0.50
U 850	0.67	0.42	0.48	0.60	0.60
V 850	-0.12	-0.10	0.06	-0.34	-0.17
W 700	-0.11	-0.09	-0.10	0.04	-0.11
q 850	-0.80	-0.18	-0.82	-0.48	-0.83

daily	PM2.5	SO_2	NO_2	netOLR	T dew
SO_2	0.08				
NO_2	0.10	0.63			
netOLR	-0.04	0.18	0.18		
T dew	-0.02	-0.32	-0.35	-0.26	
U 925	0.23	0.16	0.18	0.07	-0.28
V 925	0.14	-0.05	-0.05	-0.19	-0.14
delta T	0.17	0.18	0.19	0.30	-0.08
L.H.F.	-0.09	-0.15	-0.17	-0.09	-0.14

hourly	$PM_{2.5}$	SO_2	S.H.F.	B.L.H.	U wind
SO_2	0.00				
S.H.F.	0.06	-0.09			
B.L.H.	-0.08	-0.22	0.43		
U wind	0.13	-0.05	-0.22	0.07	
V wind	0.15	-0.31	0.11	0.44	0.70

locations, coal loading zones, and the high pollution footprint aligned to the coast.

Time series of monthly air constituents at Richards Bay over the period 2000-2023 are presented in Fig 2a, with mean annual cycles in Fig 2b-e. None of the variables contain significant trends (r^2 < 1%). Mean annual cycles are noteworthy and show peaks for SO_2 in June, for CO in July, and for O_3 in August-September. 850 hPa specific humidity at Richards Bay negatively correlates with air pollutants and shows a minimum in June-July. Table 2a summarizes the temporal cross-correlations with monthly

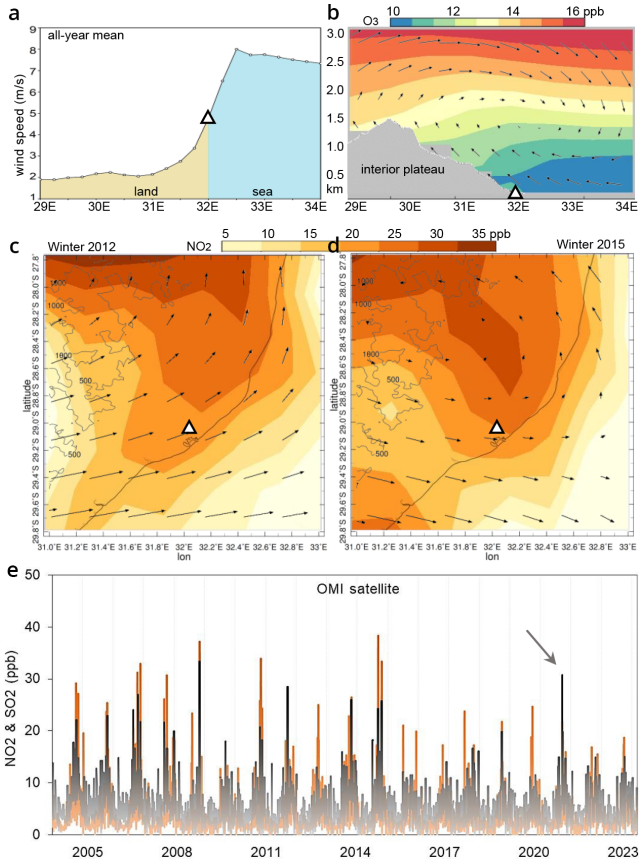

Figure 3: *West-east section on 28.8S of 2000-2023 mean: a) wind speed, b) height section of O_3 and zonal circulation (vector, max 3 m/s). Mean winter maps of OMI satellite NO_2: c) May-Aug 2012 and d) May-Aug 2015 with near-surface wind (vector, max 3 m/s). e) Temporal record of daily OMI satellite observed NO_2 (orange) and SO_2 (grey) in Richards Bay. Arrow points to case study 15-17 June 2021.*

weather conditions. $PM_{2.5}$ is quite insensitive except for U 850 wind (r = 0.42) indicating that westerlies enhance particulate dust in Richards Bay. SO_2 and CO are highly correlated (r = 0.77) and also increase under westerly winds and in dry weather (q 850 humidity, r = -0.82). Ozone behaves similarly to most air constituents except to increase with wind speed (r = 0.53) suggesting importation from distant sources. The apparent high correlation values in Table 2a derive mainly from seasonality.

Figure 3a illustrates differences in the land-sea climate along a section through Richards Bay. Surface winds over the sea exceed 7 m/s while long-term averages over the coastal plains are 2 m/s. Channelling of airflow by the South African escarpment helps maintain strong gradients in dispersion across the coast. As mentioned earlier, O_3 is a secondary trace gas formed by the oxidation of CO in the presence of NO_2 and sunlight (Ryu and Jenkins 2005, Zhang et al. 2010); it is reduced over the ocean by halogens (Read et al. 2008, Saiz-Lopez & Fernandez 2016). In Figure 3b the long-term average height section of O_3 shows an increase with height and distance from the coast. Clean marine air is swept inland by low-level easterly winds and summer-time sea breezes. The mean zonal circulation exhibits overturning, with rising motion over the Drakensberg, upper westerly winds and sinking motion over the Mozambique Channel.

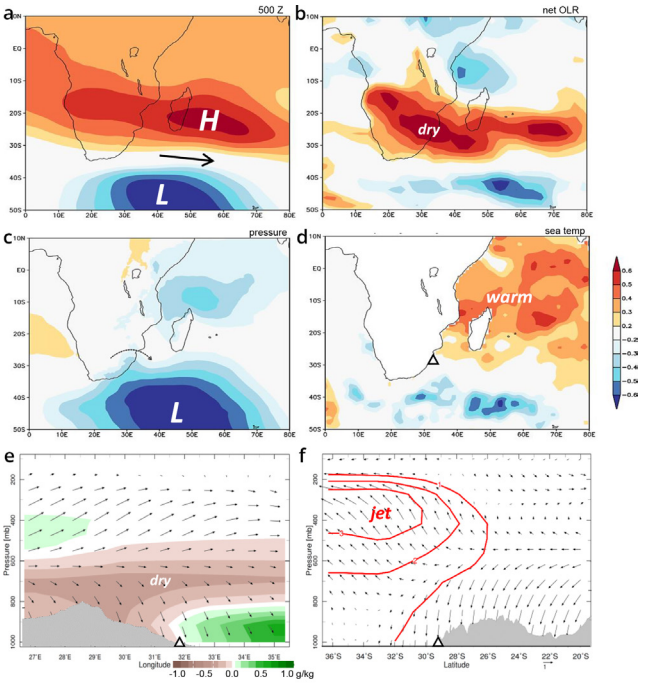

Figure 4: *Correlation of May-Aug 2000-2023 air pollution index with: a) 500 hPa geopotential height, b) satellite net OLR, c) sea level air pressure, and d) sea surface temperature, all use same scale. Composite anomalies of top 20 air pollution months: e) zonal circulation (vector, max 5 m/s) and humidity (shaded) along 28.7S, f) meridional circulation (vector, max 2 m/s) and zonal wind (contour) along 32E, with vertical motion exaggerated and elevation profile.*

Dispersion footprint and daily statistics

The winter mean maps of OMI satellite NO_2 concentrations (Fig 3c,d) reveal a footprint inland from Richard Bay that links westward to agricultural and industrial plumes from the interior. Marine air exhibits low concentrations but seldom penetrates westward during winter due to the prevailing offshore airflow. Local air quality does not exceed long-term health guidelines and is connected to nearby urban hotspots.

Figure 3e presents the daily time series of NO_2 and SO_2 which exhibits spikes due to the changeable weather. Summer values are suppressed by rainfall and unstable northeasterly winds and tend to remain below 10 ppb. During winter spells of dry weather and westerly winds daily values exceed 20 ppb. The time series have no significant trend, but year-to-year variability is evident and mainly related to the frequency of offshore (polluting) to onshore (clean) airflow.

Daily statistics are listed in Table 2b for 2004-2023. Dewpoint temperatures are associated with NO_2 and SO_2 (r = -0.35), followed by U_{925} wind and $PM_{2.5}$ (r = 0.23). Delta temperature is positively cross correlated with all air constituents (r = 0.18) and tells a story about the weather. During winters when transient frontal troughs are located to the west of Richards Bay 'berg' winds from the plateau descend, compress and dry the air. Nocturnal cooling creates a thermal inversion and shallow boundary layer that traps air pollutants, a universal phenomenon. In some winters the frontal troughs are followed by ridging high pressure cells that cleanse the air, but in other years the troughs are followed by sunny skies and continued poor dispersion. Those climatic differences are studied below.

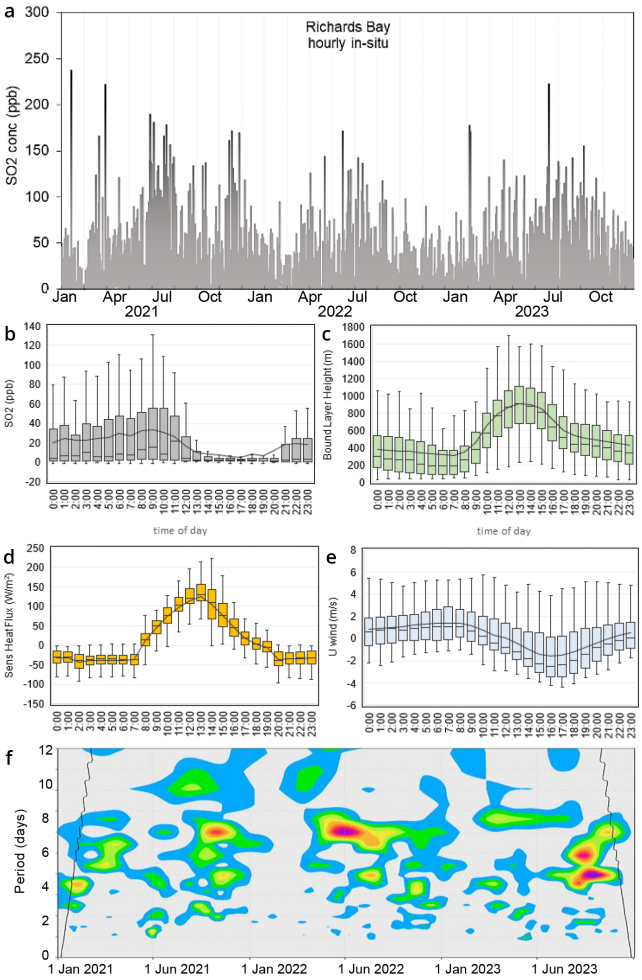

Figure 5: *a) In-situ measured hourly SO_2 concentration over three years. Mean diurnal cycle analysis during winter May-Aug 2021: b) SO_2, c) boundary layer height, d) sensible heat flux, e) east-west U wind, all times local. f) Daily dewpoint temperature wavelet spectra shaded > 90% confidence to reveal weather pulsing.*

Inter-annual variability

Using the monthly air pollution index (sum of time series in Fig 2a), point-to-field correlations illustrate the conditions distinguishing clean and polluted winters in Figure 4a-d. Warm sea temperatures in the west Indian Ocean cause a 500 hPa ridge over Madagascar 20°S, 55°E and a trough over the mid-latitudes 40°S, 40°E. A thermal wind pulls airflow over Richards Bay from the northwest, which is dry. Many of the features cover thousands of kilometers: the dry ridge extends from Namibia 15°S, 15°E to Mauritius 20°S, 60°E (Fig 4a,b), the surface low pressure extends from 35°-50°S, 30°-60°E (Fig 4c). The sea temperature pattern (Fig 4d) reflects the Indian Ocean dipole linked to slow moving ocean Rossby waves, equatorial winds and Pacific El Nino conditions (Kanyanga 2008, Nagura & McPhaden 2010, Jury 2018). Correlations are indicative of winter climate influences on local dispersion.

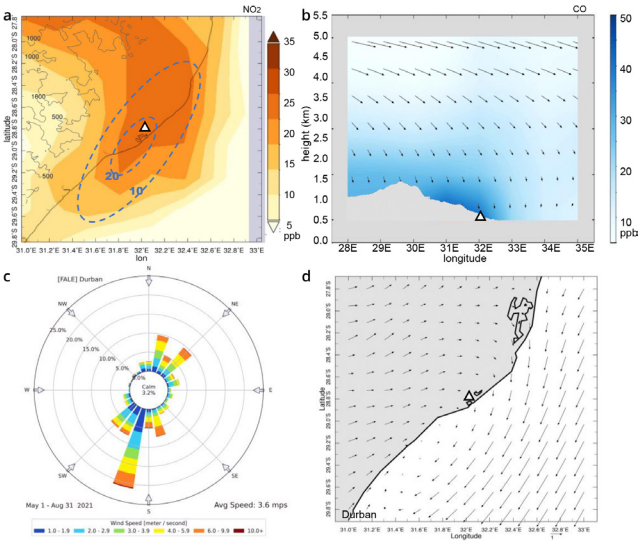

Figure 6: *Mean conditions during winter 2021. Satellite observed: a) NO_2 concentration map with $PM_{2.5}$ contours (dashed µg/m³), and b) CO height section on 28.7°S and zonal circulation (vector, max 8 m/s). c) wind rose at Durban, d) mean surface winds (vector, max 3 m/s) indicating circular airflow.*

Composite atmospheric circulation anomalies over Richards Bay during top 20 winter months with high air pollution are presented in Figure 4e,f. As expected, the zonal airflow is from west and reflects sinking motion with a dry characteristic below 500 hPa (~5.5 km) from 27°-33°E. The meridional airflow reflects poleward airflow, sinking motion below 500 hPa, and a strengthened upper level jet. A curious feature in these circulation patterns is the diffluent rising motion above 500 hPa. To the east of Richards Bay, enhanced humidity below 850 hPa remains over the Mozambique Channel under westerly winds. The downstream 'pull' by the thermal winds over the south Indian Ocean induces poor dispersion at Richards Bay.

Hourly statistics and diurnal cycle

Hourly time series of in-situ SO_2 from Jan 2021 to Dec 2023 is presented in Figure 5a, and temporal statistics for $PM_{2.5}$ and SO_2 during winter 2021 are listed in Table 2c. Spikes in the time series are attributed to diurnal oscillations amidst seasonal weather pulsing that brings rainfall. Particulates do not respond much to weather conditions except for higher U V wind correlations linked to turbulence. Boundary layer height and V wind are negatively cross-correlated with SO_2 (r = -0.22, -0.31). A shallow mixing depth and northerly winds induce poor dispersion at an hourly time scale. Amongst the weather variables, sensible heat flux and V wind are associated with boundary layer height (r = 0.43, 0.44) while U and V winds correspond (r = 0.70), merely indicating the SW-NE axis of coastal airflow.

The mean diurnal cycle averaged over winter 2021 is illustrated in Figure 5b-e. SO_2 reveals much higher values (30+ ppb) from 03:00 – 11:00 associated with nocturnal thermal inversions and shallow boundary layer height that traps pollutants below 400 m. Sensible heat fluxes are negative at night (-40 W/m²) and cool the lower atmosphere creating stability. By mid-day the sensible heat flux reaches 140 W/m² driving an alternation of U winds

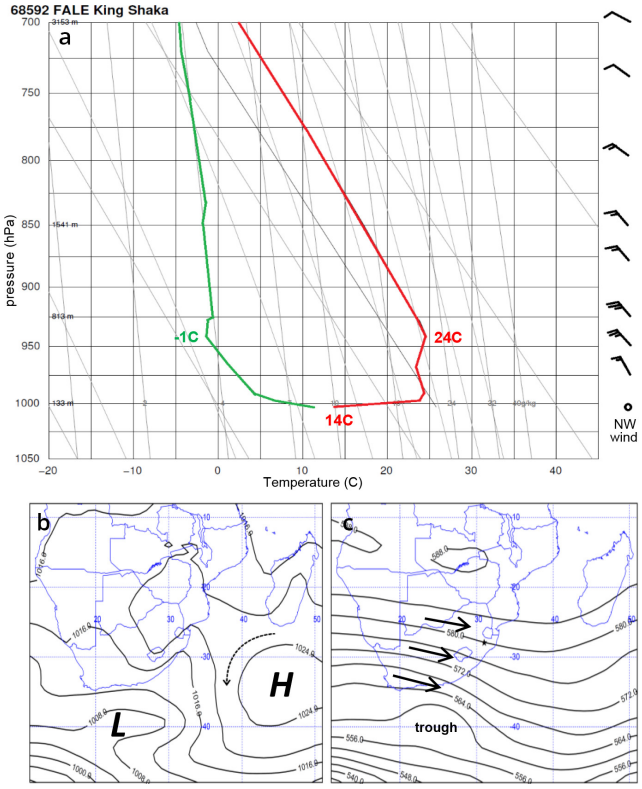

Figure 7: *Weather conditions at 02:00 16 June 2021: a) Durban radiosonde profile, b) sea level air pressure map (hPa), c) 500 hPa geopotential height map (m), with pressure cells and wind icons.*

from landbreeze (+1 m/s at 07:00) to seabreeze (-2 m/s by 16:00). The back and forth airflow tends to recirculate pollutants, as seen in the next section on mapping winter 2021 dispersion.

Figure 5f reveals weather pulsing by applying wavelet spectral analysis to the time series of ERA5 dewpoint temperature. Oscillations of 4-8 days are statistically significant, and indicate the changeable nature of coastal weather at Richards Bay.

Mapping winter 2021 dispersion

Maps of NO_2 and CO concentration over Richards Bay area are presented in Figure 6a,b for May-Aug 2021. NO_2 shows a footprint of higher values (30 ppb) over and northeast of Richards Bay. Pollutants from local urban and industrial emissions appear linked to those from the Highveld to the northwest. NO_2 is derived from combustion and thus reflects emissions from local traffic, shipping, and agricultural burning. The CO height section identifies local surface emissions that produce the highest concentrations (40 ppb) below 2 km. The zonal circulation is dominated by upper westerlies that subside and weaken toward the surface. CO emissions from Durban infiltrate the Tugela Valley near 31E, according to the winter 2021 'wind rose' in Figure 6c, which shows a 22% frequency from SSW sector. 45% of the time the winter winds are < 3 m/s and non-dispersive. Similar characteristics have been reported at Richards Bay (Petzer et al 2008). One of the most interesting outcomes of this research is the circular nature of net surface airflow (Figure 6d). Winds from the northeast characterize the marine environment, while terrestrial winds are from the southwest. The centre of this

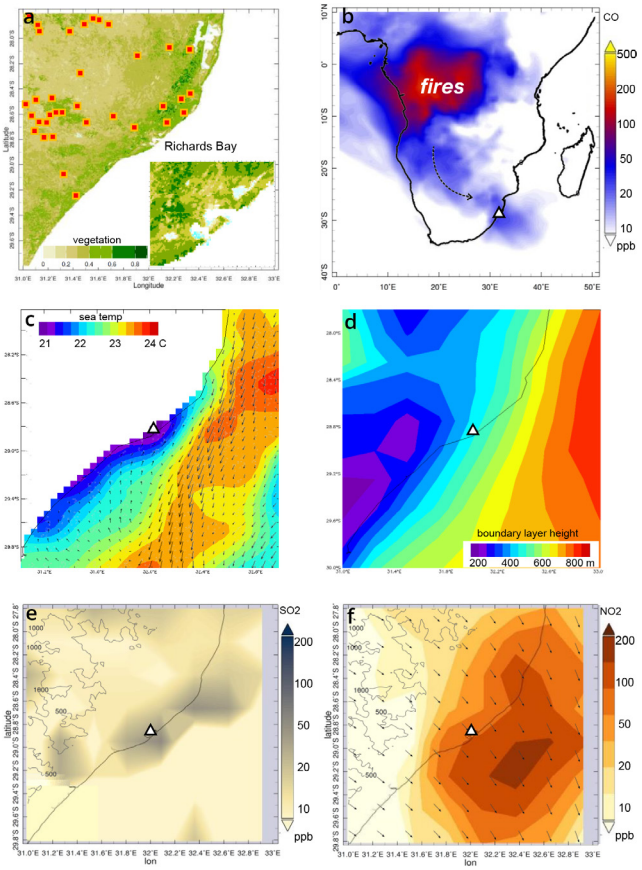

Figure 8: *Environmental conditions during an air pollution event 15-17 June 2021: a) vegetation fraction and local fires detected by satellite (inset zoomed), b) regional smoke plume CO concentration (log-scale), c) sea temperature and ocean currents, d) boundary layer height, e) SO_2 concentration (log-scale) with elevation contours, and f) NO_2 concentration and wind (vector, max 3 m/s). Triangle denotes Richards Bay.*

rotary circulation is calm and overlies Richards Bay, resulting in little net transport during winter. Although recirculation may be inferred, the ever-present weather pulsing by atmospheric Rossby waves and their attendant high and low pressure cells forces an oscillation of this rotary airflow.

Air pollution episode: 15-17 June 2021

The daily time series of NO_2 and SO_2 (cf. Fig 3e) identified 15-17 June 2021 with high concentrations representative of a winter air pollution episode. Weather conditions are analyzed beginning with the 02:00 16 June 2021 radiosonde profile at Durban (Figure 7a) 150 km southwest of Richards Bay. The most striking feature was a 10°C nocturnal inversion from 0 – 60 m that decouples momentum transfer resulting in surface winds of 1 m/s. Thermal stability continued to 500 m, but airflow from NW increased to 12 m/s indicative of 'berg' winds. Dewpoint temperatures dropped to -1°C at 500 m due to the subsidence. A lapse rate of -9°C/km above the inversion corresponded with NW winds of 6 m/s. Weather maps at the surface and 500 hPa are illustrated in Figure 7b,c and show a trough to the southwest with a surface low pressure at 40°S, 23°E. A coastal low preceded the trough and was located over the Eastern Cape on 16 June 2021, while the surface Mascarene high was at 34°S, 45°E. The

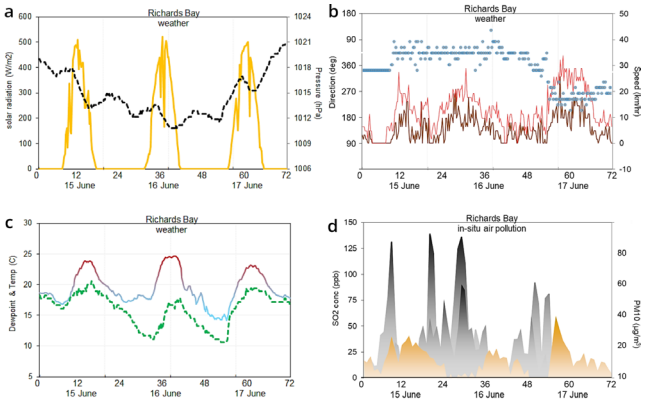

Figure 9: *Hourly in-situ weather and air pollution records during an event 15 - 17 June 2021: a) solar radiation and air pressure reduced to sea level, b) wind direction (dots), speed and gust, c) air temperature and dewpoint, and d) in-situ SO_2 (grey) and PM_{10} concentration (brown).*

upper westerly jet stream was 40 m/s, consistent with regional forcing seen in Fig 4a.

During this air pollution episode, local emissions were joined by smoke plumes from agricultural burning across Africa (Figure 8a,b). Fires over KwaZulu-Natal, the western Zambezi and the Congo Basin were entrained toward Richards Bay causing surface CO concentrations to rise. The boundary layer height was tilted by land-sea contrasts (Figure 8c,d): over the warm ocean current (Agulhas) values were 800 m, while over the cool Tugela Valley, values were 200 m. SO_2 and NO_2 concentration maps in Figure 8e,f suggest that the prevailing winter land breeze dispersed the Richards Bay emissions seaward.

In-situ station data were analyzed from 15-17 June 2021 in Figure 9a-d. Net solar radiation exhibited a diurnal cycle reaching at 500 W/m^2 at mid-day with dips from passing clouds. The air pressure of 1019 hPa on the 15th declined to 1011 hPa by the 16th then recovered to 1021 by the 17th, all indicative of passage by a coastal low associated with the mid-latitude trough. Northeasterly winds fluctuated above 10 km/hr on the 15th and 16th then became calm and switched to southwesterly on the 17th. Air temperatures warmed to 24°C each afternoon and declined to 15°C on the evening of the 16th. Dewpoint temperatures might be expected to remain steady but have diurnal cycling, with values of 11°C in the early morning of the 16th and 17th. These indicate 'berg' winds join the nocturnal land breeze and promote radiation cooling during air pollution episodes. Hourly in-situ SO_2 and PM_{10} concentrations revealed spikes above 100 ppb and 20 ug/m^3. These were out-of-phase: particulates rose during the day, whereas SO_2 rose at night. By the 17th south-westerly winds had dispersed SO_2 away from the monitoring stations and toward the city.

Particulate episode: 4-5 July 2022

Unlike trace gases, $PM_{2.5}$ and PM_{10} records do not exhibit a clear annual cycle. Long-range transport of Kalahari dust and Zambezi smoke plumes join urban emissions from the Highveld during dry spells when troughs maintain north-westerly airflow. These features appear during a case study 4-5 July 2022 in Figure

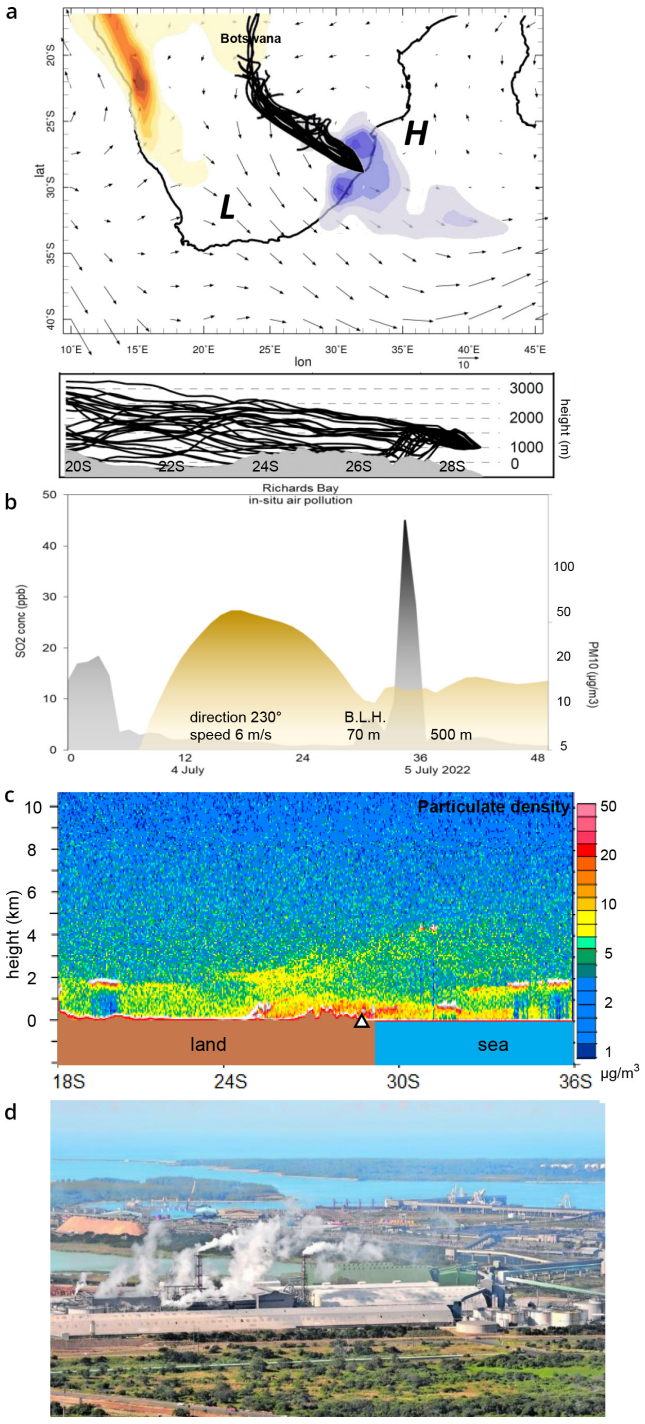

Figure 10: *a) HYSPLIT back trajectories arriving at Richards Bay 4-5 July 2022 (map and side view), MERRA2 dust (brown) and smoke (blue) plumes and 850 hPa wind (vectors). b) Hourly in-situ SO_2 (grey) and PM_{10} (brown) on 4-5 July 2022, c) N-S height section on 31.8E of satellite lidar backscatter indicating particulate density (log-scale) at 22:00 on 4 July 2022, d) aerial photo of Richards Bay industrial zone and harbour.*

10a. HYSPLIT back-trajectories arrive from the 1-3 km layer over Botswana, gathering a variety of particulates along the way.

Local measurements (Figure 10b) confirm high particulate concentrations on the afternoon of 4 July as southwest winds of 6 m/s spread coal dust from the harbour. ERA5 weather data indicate warm, dry, turbulent conditions with sensible heat fluxes of 150 W/m^2 and boundary layer height of 760 m. The CALIPSO satellite height section (Figure 10c) reveals a dense layer of particulates below 1 km and plumes slanting upward from land to sea. Local measurements contain a 45 ppb spike of SO_2 at Richards Bay at 10:00 on 5 July 2022, indicating the sudden vertical spread of elevated plumes as boundary layer height grew from 70 m at sunrise to 500 m by noon. The mixture of distant and local emissions add to the burden of respiratory health, and tend to accumulate under the same weather conditions.

Conclusions

This study has deepened our understanding of climate and weather conditions underlying Richard Bay's air pollution dispersion, based on satellite and in-situ measurements assimilated by sophisticated models. Near-surface concentrations of trace gases and particulates reach high concentrations under dry stable 'berg' winds. Temporal records of CO, NO_2, O_3, $PM_{2.5}$, and SO_2 (2000-2023) exhibit no trend and short-term dose exceedances of individual pollutants are rare and confined to winter mornings.

Regional point-to-field correlation maps of the Richards Bay winter air pollution index determined that warming in the west Indian Ocean accelerates the jet stream over Madagascar and pulls smoke- and dust-laden north-westerly winds across the South African plateau toward the coast of KwaZulu-Natal. A case study 15-17 June 2021 revealed a 10°C thermal inversion caused by a negative sensible heat flux of -40 W/m^2 during the night, leading to SO_2 concentrations above 100 ppb in the morning along the main access road (28.8°S, 32°E). In contrast, summer weather is characterized by turbulent mixing and rainfall that cleanse the air. At daily and hourly time scales, low dewpoint temperature, boundary layer height, and northwest wind best indicate poor air quality. Winter dry spells that accumulate air pollutants can be anticipated by local health services to prepare for increased respiratory impacts.

Recommendation

The proximity of Richard Bay's industrial zone to the scenic waterfront (Figure 10d) makes it difficult to conceive a mitigating strategy that could put the city on a more environmentally friendly path. Although coal exports will decline as the world seeks to limit greenhouse warming, the current use of road transport for delivery to the harbour has caused soot build-up on city streets, leading to respiratory impairment and lost productivity. Coal delivery by rail and transfer to ships on the southwest side of the harbour seems a better option.

Acknowledgements

The author visits Zululand every winter and is grateful for support from the SA Department of Higher Education and Training. Much of the air constituent and meteorology data were

drawn from websites: NASA-Giovanni, KNMI Climate Explorer, IRI Climate Library, APDRC-Hawaii, Univ Wyoming radiosonde, IEM wind rose, and Wundermap. A spreadsheet is available on request.

References

Akimoto, H. 2003, Global air quality and pollution, S. Afr. J. Science, 302, 1716–1719. https://doi.org/10.1126/science.1092666

Bhattachan, A., D'Odorico, P., Baddock, M., Zobeck, T., Okin, G. & Cassar, N., 2012, The southern Kalahari: a potential new dust source in the Southern Hemisphere? Environ. Res. Letters 7, doi10.1088/1748-9326/7/2/024001. https://doi.org/10.1088/1748-9326/7/2/024001

Bucsela, E.J., Krotkov, N.A., Celarier, E.A., Lamsal, L.N., Swartz, W.H., Bhartia, P.K., Boersma, K.F., Veefkind, J.P., Gleason, J.F. & Pickering, K.E., 2013, A new stratospheric and tropospheric NO_2 retrieval algorithm for nadir-viewing satellite instruments, applications to OMI, Atmos. Meas. Tech. 6, 2607–2626. https://doi.org/10.5194/amt-6-2607-2013

Burrows, J.P., Platt, U. & Borrell, P. (eds.), 2011, The Remote Sensing of Tropospheric Composition from Space, Springer-Verlag, Berlin, 536 pp. https://doi.org/10.1007/978-3-642-14791-3

Conradie, E.H., van Zyl, P.G., Pienaar, J.J., Beukes, J.P., Galy-Lacaux, C., Venter, A.D. & Mkhatshwa, G.V., 2016, The chemical composition and fluxes of atmospheric wet deposition at four sites in South Africa, Atmos. Environ., 146, 113-131. https://doi.org/10.1016/j.atmosenv.2016.07.033

Diab, R. & Matooane, M., 2003, Health risk assessment for sulphur dioxide pollution in south Durban, South Africa, Arch. Environ. Health 58, 12. https://doi.org/10.3200/AEOH.58.12.763-770

FIRMS, 2023, Fire information resource management system accessed: https://firms.modaps.eosdis.nasa.gov

Gelaro, R. & 30 co-authors, 2017, The modern-era retrospective analysis for research and applications, v2 (MERRA-2), J. Climate 30, 5419-5454. https://doi.org/10.1175/JCLI-D-16-0758.1

GEOS-5, 2016, data assimilation system accessed via: https://gmao.gsfc.nasa.gov/pubs/docs/GEOS-5.0.1_Documentation_r3.pdf

Gopaul, A., Friedrich, E. & Stretch, D. 2019, Public transportation and greenhouse gas emissions: a case study of the eThekwini municipality South Africa, Curr. Trends Civil & Struc. Eng. 3, doi10.33552/CTCSE.2019.03.000553. https://doi.org/10.33552/CTCSE.2019.03.000553

Hersbach, H. & 19 co-authors, 2020. The ERA5 global reanalysis, Quart. J. Roy. Meteor. Soc., 146, 1999-2049.

Hersey, S.P., Garland, R.M., Crosbie, E., Shingler, T., Sorooshian, A., Piketh, S.J. & Burger, R. 2015, An overview of regional and local characteristics of aerosols in South Africa using satellite, ground, and modeling data, Atmos. Chem. Phys. 15, 4259-4278. https://doi.org/10.5194/acp-15-4259-2015

IEM, 2021, Iowa Environmental Mesonet, Wind rose analysis from Durban airport, accessed via: mesonet.agron.iastate.edu/sites/windrose.phtml?station=FALE&network=ZA__ASOS

Jaggernath, J. 2013, A socio-economic and spatial investigation into the health implications of air pollution in Richards Bay, South Africa, PhD thesis, Univ KZN Durban, researchspace.ukzn.ac.za

Josipovic, M., Annegarn, H.J., Kneen, M.A., Pienaar, J.J. & Piketh, S.J., 2011, Atmospheric dry and wet deposition of sulphur and nitrogen species and assessment of critical loads of acidic deposition exceedance in South Africa. S. Afr. J. Science, 107, 1-10. https://doi.org/10.4102/sajs.v107i3/4.478

Jury, M.R., 2000, Determination of health impacts in urban regions exposed to atmospheric pollutants, Clean Air J. 10, 7-13. https://doi.org/10.17159/caj/2000/10/6.7096

Jury, M.R. & Guyot, S. 2009, Environmental services and development in an African port city, Science Res. Essays, 4, 1370-1380.

Jury, M.R., 2017, Statistics and meteorology of air pollution episodes over the South African Highveld based on satellite-model datasets, J. Appl. Meteor. Climatol., 56, 1583-1594. https://doi.org/10.1175/JAMC-D-16-0354.1

Jury, M.R., 2018, South Indian Ocean Rossby waves, Atmos. Ocean, 56, 322-331. https://doi.org/10.1080/07055900.2018.1544882

Jury, M.R. & Buthelezi, M. 2022. Air pollution dispersion over Durban South Africa, Atmosphere MDPI, doi:10.3390/atmos13050811. https://doi.org/10.3390/atmos13050811

Kanyanga, J.K., 2008, El Nino Southern Oscillation and atmospheric aerosol transport over southern Africa. PhD thesis, Univ. Witwatersrand, 212 pp.

Korhonen, K. & 17 co-authors, 2014, Atmospheric boundary layer top height in South Africa: measurements with lidar and radiosonde compared to three atmospheric models, Atmos. Chem. Phys., 14, 4263-4278. https://doi.org/10.5194/acp-14-4263-2014

Krotkov, N., Carn, S., Krueger, A., Bhartia, P. & Yang, K., 2006, Band residual difference algorithm for retrieval of SO_2 from the Aura Ozone Monitoring Instrument (OMI), IEET Geosci. Rem., 44, 1259-1266. https://doi.org/10.1109/TGRS.2005.861932

Krotkov, N.A. & 17 co-authors, 2016, Aura OMI observations of regional SO_2 and NO_2 pollution changes from 2005 to 2015, Atmos. Chem. Phys., 16, 4605-4629. https://doi.org/10.5194/acp-16-4605-2016

Lamsal, L.N. & 14 co-authors, 2014, Evaluation of OMI operational standard NO_2 column retrievals using in situ and surface-based NO_2 observations, Atmos. Chem. Phys., 14, 11587-11609. https://doi.org/10.5194/acp-14-11587-2014

Lourens, A.S.M., Beukes, J.P., vanZyl, P.G., Fourie, G.D., Burger, J.W., Pienaar, J.J., Read, C.E. & Jordaan, J.H., 2011, Spatial and temporal assessment of gaseous pollutants in the Highveld of South Africa. S. Afr. J. Science, 107, 1-8. https://doi.org/10.4102/sajs.v107i1/2.269

Ma, X., Bartlett, K., Harmon, K. & Yu, F., 2013, Comparison of AOD between CALIPSO and MODIS: significant differences over major dust and biomass burning regions, Atmos. Meas. Tech., 6, 2391-2401. https://doi.org/10.5194/amt-6-2391-2013

Magi, L.M. & Nzama, T.A. 2002, Perspectives of recreation and tourism geographies in South Africa, South Afr. Geogr. J., 84, 67-76. https://doi.org/10.1080/03736245.2002.9713757

Mitchell, J., Jury, M.R. & Mulder, G. 2005, A study of Maputaland beach dynamics, South Afr. Geogr. J., 87, 43-51. https://doi.org/10.1080/03736245.2005.9713825

Mehlhorn, P., Viehberg, F., Kirsten, K., Newman, B., Frenzel, B., Gildeeva, O, Green, A., Hahn, A. & Haberzettl, T. 2021, Spatial distribution and consequences of contaminants in harbour sediments, A case study from Richards Bay Harbour, South Africa, Marine Pollution Bulletin, 172, 112764. https://doi.org/10.1016/j.marpolbul.2021.112764

Molod, A., Takacs, L., Suarez, M. & Bacmeister, J. 2015, Development of the GEOS-5 atmospheric general circulation model: evolution from MERRA to MERRA2, Geosci. Model Dev. 8, 1339-1356. https://doi.org/10.5194/gmd-8-1339-2015

Nagura, M. & McPhaden, M.J. 2010, Dynamics of zonal current variations associated with the Indian Ocean dipole, J. Geophys. Res., 115, C11026, doi:10.1029/2010JC006423.

Okello, N.O., Camminga, S., Okello, T.W., Zunckel, M., 2018, Spatial and temporal trends of PM_{10} and SO_2 in the Richards Bay Area, Clean Air J., 28, 80-89. https://doi.org/10.17159/2410-972x/2018/v28n2a20

Okello, N.O., Okello, T.W. & Zunckel, M. 2020, Public perceptions of air quality status and suggestions for improvement: The case of Richards Bay ... South Africa, Clean Air Journal, 30, https://doi.org/10.17159/caj/2020/30/1.8001

Petzer, G., Liebenberg, H., Thomas, R., & Burger. L.W., 2008, Air quality impact assessment … in Umhlathuze, APP/08/CTR-01, Airshed Planning, 98pp., etc-africa.co.za/attachments/article/202/

Piketh, S.J., Annegarn, H.J. & Tyson, P.D., 1999, Lower tropospheric aerosol loadings over South Africa: The relative contribution of aerosol dust, industrial emissions, and biomass burning. J. Geophys. Res., 104, 1597-1607. https://doi.org/10.1029/1998JD100014

Randles, C.A., da Silva, A.M., Buchard, V., Colarco, P.R., Darmenov, A., Govindaraju, R., Smirnov, A., Holben, B., Ferrare, R., Hair, J., Shinozuka, Y. & Flynn, C.J. 2017, The MERRA-2 aerosol reanalysis, 1980 onward: system description and data assimilation evaluation, J. Climate 30, 6823-6850. https://doi.org/10.1175/JCLI-D-16-0609.1

Read, K.A. and 15 co-authors. 2008, Extensive halogen-mediated ozone destruction over the tropical Atlantic Ocean. Nature Letters, 453, 1232-1235. https://doi.org/10.1038/nature07035

Ryu, J-H. & Jenkins, G.S. 2005, Lightning-tropospheric ozone connections: EOF analysis of TCO and lightning data. Atmos. Environ. 39, 5799-5805. https://doi.org/10.1016/j.atmosenv.2005.05.047

Saiz-Lopez, A. & Fernandez, R.P. 2016, On the formation of tropical rings of atomic halogens: Causes and implications. Geophys. Res. Lett., 43, 2928–2935. https://doi.org/10.1002/2015GL067608

SAAQIS, 2023, South African Air Quality Information System, data access.

Scorgie, Y, 2012, Urban air quality management and planning in South Africa, PhD Thesis, Univ Johannesburg, 333 pp.

Shikwambana, L.D., & Sivakumar, V. 2019, Investigation of various aerosols over different locations in South Africa using satellite, model simulations and LIDAR. Meteo. Appl. 26, 275-287. https://doi.org/10.1002/met.1761

Simpson, A.J. & McGee, O.S. 1996, Analysis of the fumigation effect on pollutants over Pietermaritzburg, S. Afr. Geogr J., 78, 41-46. https://doi.org/10.1080/03736245.1996.9713605

Stein, A.F., Draxler, R.R, Rolph, G.D., Stunder, B.J.B., Cohen, M.D., Ngan, F., 2015, NOAA's HYSPLIT atmospheric transport and dispersion modeling system, Bull. Amer. Meteor. Soc., 96, 2059-2077. https://doi.org/10.1175/BAMS-D-14-00110.1

Tularam, H., Ramsay, L.F., Muttoo, S., Brunekreef, B., Meliefste, K., deHoogh, K. & Naidoo, R.N., 2021, A hybrid air pollution / land use regression model for predicting air pollution concentrations in Durban, South Africa, Environ. Poll. 274/ https://doi.org/10.1016/j.envpol.2021.116513

Winker, D.M., Hunt, W.M. & McGill, M.J., 2007, Initial performance assessment of CALIOP, Geophys. Res. Lett., 34, L19803. https://doi.org/10.1029/2007GL030135.

World Bank, 2016, The cost of air pollution: strengthening the economic case for action. Washington, D.C., World Bank Group. 122 pp.

World Health Organization, 2021, WHO global ambient air pollution database, accessed via: www.who.int/data/gho/data/themes/air-pollution/who-air-quality-database#

Zhang, L., Jacob, D.J., Liu, X., Logan, J.A., Chance, K., Eldering, A. & Bojkov, B.R. 2010, Intercomparison methods for satellite measurements of atmospheric composition: application to tropospheric ozone from TES and OMI, Atmos. Chem. Phys., 10, 4725–4739. https://doi.org/10.5194/acp-10-4725-2010